UCRL - 73974
PREPRINT

CONF-720707--10

LAWRENCE LIVERMORE LABORATORY
University of California/Livermore, California

X-RAY-INDUCED PHOTOCONDUCTIVITY IN DIELECTRIC FILMS

R. C. Weingart
R. H. Barlett
R. S. Lee
W. Hofer

June 16, 1972

This paper was prepared for presentation at the
IEEE Annual Conference on Nuclear and Space Radiation Effects,
Seattle, Washington, July 24-27, 1972

X-RAY-INDUCED PHOTOCONDUCTIVITY IN DIELECTRIC FILMS*

R. C. Weingart, R. H. Barlett, and W. Hofer

University of California, Lawrence Livermore Laboratory
Livermore, California 94550

R. S. Lee

Kansas State University
Manhattan, Kansas

ABSTRACT

We have measured the conductivity induced in films of polyethylene, epoxy, polytetrafluoroethylene, polyethylene terephthalate, polyimide, and glass by x rays at dose rates between 10^9 and 10^{10} rads/sec (dose in air). The films were 0.05 to 1.25 mm thick. The x-ray spectrum peaked in the vicinity of 10 keV, and the x-ray pulse width was about 40 nsec FWHM. X-ray-induced photocurrents were found to obey Ohm's law at low bias voltages (less than 1 kV). Above 1 kV, however, we observed that the peak photoconductivity signals from some of the 0.05-mm-thick materials began to increase at a slightly faster than linear rate with bias voltage. The glass samples exhibited no apparent delayed conductivity, while the other sample materials showed various amounts. The magnitude of the delayed conductivity in polytetrafluoroethylene, polyethylene terephthalate, and polyimide depended on the electric field, an effect that is consistent with Poole-Frenkel

*Work performed under the auspices of the U.S. Atomic Energy Commission.

field-assisted carrier generation. We have qualitatively described the magnitude and time dependence of the conductivity signals by a simple trapping model using reasonable values for mobility, trap density, capture cross sections, and trap depths.

INTRODUCTION

When the electrical components and circuitry of a warhead are exposed to a nuclear radiation environment, induced voltages and currents are generated that may be large enough to damage critical components and disable the warhead. In our continuing program at LLL to understand the mechanisms by which these voltages and electrical currents are generated, we are making careful laboratory measurements of charge emission from material surfaces[1] as well as the charge displacement effects that occur within the bulk of an insulating layer under x-ray exposure. We are attempting to use this data in computer models to explain the complex signals observed from cables and other electrical components in nuclear effects tests. The radiation induced conductivity in the dielectrics of these components is an essential parameter in the analysis of these signals.

We have measured the radiation induced conductivity of films of polyethylene terephthalate, polyimide, polytetrafluoroethylene, polyethylene, epoxy, and glass at dose rates near 10^{10} rads/sec (air). Previous experimental data on conductivity at these and higher dose rates is sparse and varies significantly among investigators. Our measured data on polytetrafluoroethylene is several orders of magnitude smaller than that tabulated in the TREE handbook.[2] Data on conductivity measured as a function of time and energy deposition rate in the sample is even more sparse.

The increase in conductivity that occurs in an insulating material exposed to ionizing radiation is attributed to an increase in the density of free carriers due to the excitation of electrons into the conduction band of the material. This increase in conductivity, which may be many orders of magnitude larger than the unirradiated or "dark" value, is called photoconductivity. We have measured the photoconductivity of insulating films by applying a bias voltage (to electrodes vacuum deposited on both surfaces of the film) and observing the current flowing through the sample during and after exposure to a pulse of radiation. The conductivity was obtained as a function of time and dose rate during and after the radiation pulse by using a circuit analysis code that calculates the conductivity approximately every 2 nsec.

The electrodes deposited on the insulating materials were only 500 to 2500 Å thick so that x-ray attenuation and any local dose enhancement due to electron emission from the electrodes into the film would be minimized. The thickness of the insulating samples ranged from 0.05 to 1.25 mm. The bias voltage applied acrosa the sample varied over a 5-kV range: from -2.5 to +2.5 kV. The resulting electric fields in the thinnest samples reached 5×10^5 V/cm.

We found that considerable care had to be taken in the design of the environment in which the photoconductivity measurements were made. X-ray-induced charge emission from surfaces in the vicinity of the sample as well as from the sample electrodes can contribute signals large enough to completely mask the real conductivity signal. We reduced extraneous signals to an acceptable level by covering all exposed surfaces, including the sample electrodes, with beryllium foil.

THEORY

Photoconductivity of Crystalline Semiconductors and Insulators

When a semiconductor or insulator is irradiated with electromagnetic radiation, the electrical conductivity may increase by many orders of magnitude. This phenomenon is called photoconductivity. Experiments utilizing the Hall effect have demonstrated that photoconductivity is due primarily to an increase in the free carrier densities, rather than to a change in carrier mobility. Photoconductivity occurs when the energy of the incident radiation is sufficient to excite electrons into the conduction band. Excitation may take place from the valence band or from filled eletronic levels within the band gap. Both the electrons and the holes created in this process may contribute to the conductivity.

Let n_0, p_0 be the concentration of free electrons and holes in the photoconductor in the absence of radiation and δn, δp be the increase in concentration of free electrons and holes when the photoconductor is irradiated. Then

$$n_r = n_0 + \delta n$$

$$p_r = p_0 + \delta p, \tag{1}$$

where n_r, p_r are the total concentrations of free electrons and holes during irradiation. The conductivity then becomes

$$\sigma = (n_0 \mu_e + p_0 \mu_h)e + (\delta n \mu_e + \delta p \mu_h)e$$

$$= \sigma_0 + \delta\sigma . \tag{2}$$

Accordingly, the current density $\vec{j}$ may be written in two terms:

$$\vec{j} = \sigma_0 \vec{E} + \delta\sigma\vec{E} \ , \tag{3}$$

where $\sigma_0\vec{E}$ is called the dark current and $\delta\sigma\vec{E}$ is called the photocurrent. In good insulating materials the dark current is completely negligible compared with the photocurrent except possibly at very low irradiation levels, so Eq. (3) becomes

$$\vec{j} \approx \delta\sigma\vec{E}. \tag{4}$$

Two-Level Model of a Photoconductor

Let us first examine the simplest possible model for a crystalline photoconductor.[3] Consider a solid with a completely filled valence band separated by a energy gap $\mathcal{E}_g$ from an empty conduction band. Assume that $\mathcal{E}_g$ is large enough that thermal excitation of electrons from the valence band to the conduction band may be neglected. Let electrons be excited across the gap into the conduction level at a rate g(t), leaving behind free holes in the valence band. The rate of change of electron concentration in the conduction band during irradiation is given by

$$\frac{dn}{dt} = g(t) - \alpha pn \ , \tag{5}$$

where g(t) is the generation rate of free electron-hole pairs per unit volume and αpn is the recombination rate per unit volume, which is proportional to the product of free electron and hole concentrations. From the kinetics of

the recombination process, the lifetime τ of an electron (or hole) in the conduction (or valence) band is

$$\tau = \frac{1}{\alpha p} \ . \tag{6}$$

Since the number of free electrons and free holes is the same, Eq. (5) in the steady state becomes

$$\frac{dn}{dt} = 0 = g - \alpha n_{\infty}^{2} \ , \tag{7}$$

yielding

$$n_{\infty} = \left(\frac{g}{\alpha}\right)^{\frac{1}{2}} \ , \tag{8}$$

where n_{∞} is the steady state concentration of electrons.

Since the generation rate g(t) is proportional to the energy deposition rate (dose rate), this model predicts that the steady state concentration of free carriers will vary as the square root of the dose rate. Conductivity is proportional to the free carrier concentration; thus,

$$\sigma \propto \left(\frac{\dot{\gamma}}{\alpha}\right)^{\frac{1}{2}} \ , \tag{9}$$

where $\dot{\gamma}$ is the dose rate (energy deposited per gram of material per unit time by the radiation).

Experimentally, a square root dependence of the photoconductivity on dose rate, as in Eq. (9), is rarely observed. In most materials, the dependence

of photoconductivity on dose rate is nearly linear. Also, the measured photoconductivity is many orders of magnitude smaller than that predicted by Eqs. (8) and (9).

The response time of a photoconductor is defined as the time required for the free carrier density of the photocurrent to drop to some fraction, say 0.5, of its initial value when the radiation is turned off. When $g = 0$, we obtain from Eq. (5)

$$\frac{dn}{dt} = -\alpha n^2 . \tag{10}$$

Integrating this expression, one obtains

$$n(t) = \frac{n_\infty}{1 + \alpha n_\infty t} , \tag{11}$$

where n_∞ is the steady state free carrier density at the time the exciting radiation is turned off. The response time, T, from Eq. (11) and our definition above is

$$T = \frac{1}{\alpha n_\infty} . \tag{12}$$

Using Eq. (6) and the identity of n and p we see that

$$T = \tau . \tag{13}$$

Thus, the response time and the lifetime of a free carrier in this simple model of a photoconductor are one and the same. We would expect, therefore, that a sensitive photoconductor (large n for a given g) show a long free

carrier lifetime and, from Eq. (13), a sluggish or long response time. However, this identification of response time with carrier lifetime is not observed. Many insensitive photoconducting materials with carrier lifetimes estimated to be in the 10^{-10} sec range show response times of the order of seconds. We must conclude that this simple two-level model is not in accord with experiment, and therefore we must find a more realistic model of the photoconductor.

Trapping Model of a Photoconductor

Trapping levels provide the key to a more successful model. Traps are localized states existing within the band gap of a solid. Electrons or holes captured in shallow trapping levels may be subsequently released as free carriers by thermal processes. Many of the important effects of these trapping levels may be examined in a simple model.

Consider a crystal with four energy levels, as shown in Fig. 1. The conduction and valence bands are treated as single, highly degenerate levels, since the overwhelming majority of free carriers will have energies within kT of the band edges.

Electrons are excited across the band gap at a rate g(t) from the valence level at $\mathcal{E}_v$ into the conduction level at $\mathcal{E}_c$. Let the holes arising from the excitation process be immediately captured into the electron level at $\mathcal{E}_r$ (which is filled before the exciting radiation begins). These captured holes will subsequently serve as recombination centers for free electrons. Since we assume the holes are trapped immediately we will neglect their contribution to the conductivity. The electron energy levels located at $\mathcal{E}_t$ (which are empty before the radiation strikes the sample) can capture electrons from

the conduction level and later release them back into the conduction level by a thermal exchange. These levels at $\mathcal{E}_t$ are the shallow trapping levels. We assume that they communicate only with the conduction level because of their proximity to the conduction level. The trapping and recombination levels are shown as broken lines to indicate that these energy levels do not extend throughout the crystal and hence cannot support an electrical current. Similar models have been discussed by many investigators.[4]

The allowed electron transitions are shown by the arrows in Fig. 1. The rate constant for electron capture into the trap level is α_1, that for thermal release from the trap α_2, and that for recombination α_3. The degeneracy of the conduction level, the density of trapping levels, and the density of recombination levels are N_c, N_t, and N_r, respectively. The rate constants are defined such that the probability per unit time of a transition to some new level is the product of the rate constant for the transition and the density of empty states in the new level.

Using the definitions above we can write the equations that govern the electron population in the conduction level, n_c, and in the trapping level, n_t:

$$\frac{dn_c}{dt} = g(t) - \alpha_1 n_c(N_t - n_t) + \alpha_2 n_t(N_c - n_c) - \alpha_3 n_c(n_c + n_t) \tag{14}$$

$$\frac{dn_t}{dt} = \alpha_1 n_c(N_t - n_t) - \alpha_2 n_t(N_c - n_c). \tag{15}$$

For the moment we are concerned with the steady state, in which the rate of capture of conduction electrons by the traps is equal to the rate of thermal

release of trapped electrons back into the conduction level. Therefore, in the steady state these rates of exchange exactly cancel and we may write

$$\frac{dn_c}{dt} = 0 = g(t) - \alpha_3 n_c(n_c + n_t) , \tag{16}$$

where α_3 is the rate constant for direct electron-hole recombination, $n_c + n_t$ is the number of trapped holes, and $g(t)$ is the generation rate of free electron-hole pairs. The free electron concentration in the steady state, n_c, is given by

$$n_c(n_c + n_t) = \frac{g(t)}{\alpha_3} . \tag{17}$$

There are two limiting cases of interest, depending on the relative electron concentration in the conduction level and in the trapping level. When $n_c << n_t$ we have

$$n_c = \frac{g(t)}{\alpha_3 n_t} ; \tag{18}$$

and since the generation rate $g(t)$ is proportional to the dose rate $\dot{\gamma}$ we see that

$$n_c \propto \frac{\dot{\gamma}}{\alpha_3 n_t} , \qquad [n_c << n_t] \tag{19}$$

When $n_c >> n_t$ we obtain

$$n_c \propto \left(\frac{\dot{\gamma}}{\alpha_3}\right)^{\frac{1}{2}} . \qquad [n_c >> n_t] \tag{20}$$

For trap depths greater than a few kT and level densities N_t and N_c approximately equal, Eq. (19) predicts many fewer carriers than that suggested by the bimolecular model [Eq. (8)], giving rise to photocurrents more in accord with those measured experimentally. Trap densities in our materials are estimated to be in the 10^{18} to 10^{19} cm^{-3} range, and thus a large electron population in the trap level is not unreasonable. Depending on details of the trapping level structure, the exponent of $\dot{\gamma}$ can take on values between 0.5 and 1.0.[4,5] More recently, Rose[6] has shown that a somewhat more elaborate level structure in the band gap can give rise to values of the exponent exceeding unity.

The presence of traps also accounts for the great inequality between the response time of a photoconductor and the carrier lifetime. After the radiation producing the photoconductivity is turned off, a significant conductivity may persist in the solid for times much longer than the lifetime of photoexcited carriers. This phenomenon, known as delayed conductivity, is due to thermal reemission of carriers from traps into the conduction band, where they are free to contribute to the conductivity until they recombine with trapped holes (in our model) or become trapped once again. A solid with deep trap levels, for which the probability of thermal excitation is small, would be expected to show small delayed photocurrents that persist long after the exciting radiation is turned off. The delayed conductivity may also be expected to depend on the temperature, since the rate of emission from the traps is a thermal process. If the trap levels are close to the conduction band, the temperature dependence of the photoconductivity both during and after the radiation pulse may be very large.[7]

Application of Band Theory to Amorphous and Polymeric Solids

The band theory of solids was developed to describe the behavior of crystalline solids. Although it has not been explicitly stated above, many of the important features of band theory (e.g., the existence of band gaps) arise as a result of the periodic lattice potential in the electron Hamiltonian that describes the system. In a truly amorphous solid, an ordered arrangement of atoms may not exist even over distances comparable to a few atomic spacings. Amorphous materials have been the object of intense experimental and theoretical investigation in recent years. A model proposed by Gubanov[8] and Banyai[9] describes conduction in amorphous solids in a fairly realistic manner. Mott[10] has given this model extensive theoretical development. He suggests that the essential features of band theory may be applied to amorphous solids subject to two modifications:

1) For disordered structures the band gap is replaced by a "pseudogap" or minimum in the density of electronic states.

2) Electron states in this pseudogap may be strongly localized, so they cannot contribute to the conductivity except through processes like thermal excitation. In this sense the pseudogap behaves in the same manner as a true band gap as far as electrical conduction is concerned.

Polymeric solids are highly ordered along the direction of a polymeric chain but are highly disordered compared with single-crystal or polycrystalline material. The application of band theory to polymeric solids is more obvious than for amorphous materials. The long polymer molecular may be regarded as a linear lattice. Because the intermolecular interactions are very small except between neighboring molecules in a polymer chain, it is common to

see very narrow energy bands - with widths of the order of a few kT at room temperature.[11] These very narrow bands impose special requirements on the transport of electrons or holes from a metal electrode into a polymeric insulator.

Most insulating materials of technological importance either have an amorphous structure (glasses) or are organic polymers. The electronic properties of these materials may be understood in terms of band theory subject to the limitations discussed above; namely, that we replace the band gap by a "pseudogap" in a discussion of amorphous material and that the energy bands in organic polymers are usually much narrower than in crystalline materials. Amorphous and polymeric materials exhibit the same trapping phenomena that are observed in crystalline photoconductors. The small observed photocurrents indicate high trap concentrations (estimated to be at least 10^{18} cm^{-3}) in typical amorphous and polymeric insulators.

Electrode Effects[12]

The observed photoconductivity may depend on the ability of the electrodes attached to the specimen to remove or supply charge carriers. This is a particularly difficult problem when photoconductivity measurements are attempted in highly insulating specimens under steady state irradiation. If the photoexcited carriers cannot be removed at one electrode and replenished at the other, the application of an electric field and resulting photocurrents result in a separation of positive and negative charge within the sample. The charge separation produces an electric field within the sample that opposes the applied field and eventually reduces the photocurrent to zero. This effect in the study of photoconductivity is known as polarization. It should

not be confused with dielectric polarization, in which charge separation occurs on an atomic scale under the action of an electric field. We believe that polarization effects in our experiments are minimal because the total photoconductive charge transfer that occurs during the radiation pulse is small compared with the initial charge on the electrodes of the specimen.

EXPERIMENTAL PROCEDURE

X-Ray Source

The x-ray source used for this investigation is of a design by Blumlein.[13] The x-ray burst produced by this machine is approximately 40 nsec FWHM in duration. A 0.001-in.-thick aluminum absorber placed in the beam filters out the very low energy components of the x-ray spectrum. The spectral distribution, which we measured with a bent-crystal spectrometer, is shown in Fig. 2. To measure the x-ray flux scattered by the pyrolytic graphite crystal in the 4-40 keV energy range, we used both photographic film and an array of thermoluminescent detectors. The spectrometer was calibrated by comparison with dc x-ray sources of known energy and intensity.[14,15] The spectrum consisted of characteristic x-ray lines arising from the M-to-L transitions in the tungsten anode superimposed on a bremsstrahlung spectrum.

The average dose per pulse measured at the sample location in air was 270 rads ±15%. The variation of the dose over the sample was approximately 20% – the dose falls off near the periphery of the sample. The dose was determined by averaging the readings of a number of thin LiF detectors that were exposed at the sample position.

When taking photoconductivity data, we monitored each pulse from the generator by measuring the electron emission from a thin beryllium foil

placed ahead of the sample in the path of the x-ray beam. A bias voltage applied to the foil minimized electron transit time. We assumed that the monitor signal was proportional to the rate of energy deposition in the sample; thus, the monitor enabled us to make corrections to the data for pulse-to-pulse variations in the dose due to fluctuations in the output of the generator. We also used this signal to make a time correlation between the dose rate and the photoconductive response of the sample.

In addition to random pulse-to-pulse variations in the output of the generator (±10%), we observed early in the program a steady decrease in the dose delivered to our samples with succeeding pulses. This decrease in output was found to be due to vaporized material from the anode and cathode of the generator, which was deposited on a beryllium window through which the x rays passed on their way to the sample. After about 20 pulses, sufficient tungsten and steel was deposited on this window to reduce the dose delivered to the sample by about 20%. We controlled this buildup of material by replacing a 0.005-in. beryllium insert in front of the window after each 10 or 15 pulses.

Sample Environment

Measurement of x-ray-induced photoconductivity requires great care in the design of the sample environment. Electrical noise from the pulsed x-ray source and signals due to x-ray-induced charge emission from surfaces within the sample chamber can contribute signals so large that the true photoconductivity signal cannot be extracted from the extraneous signals.

All photoconductivity measurements were made with the sample chamber evacuated to a pressure of about 10^{-4} Torr. Measurements made at pressures

higher than 10^{-1} Torr gave large signals due to air ionization and charge emission from the air onto the sample electrodes.

Figure 3 is a schematic diagram of the sample chamber. We enclosed the sample in a double-walled conducting enclosure to suppress electrical noise. Electrical contact to the sample electrodes (evaporated aluminum) was made by the collimator at the front side of the sample and by the beam stop at the rear of the sample. We designate the front side of the sample as the side closest to the x-ray source. The collimator exposed an area of the sample 2.67 cm in diameter to the x rays. The beam stop behind the sample prevented the x rays from reaching the rear of the chamber.

Figure 4 is a cross-sectional view of the collimator, the central portion of the sample, and the beam stop. Both surfaces of the collimator and both surfaces of the beam stop were covered with beryllium to minimize electron emission back into the sample chamber and into the sample. The collimator and beam stop were 2.54-mm aluminum backed by 0.254-mm gold.

X-ray-induced electron emission from surfaces within the sample chamber contains two components. One component consists of photoelectrons and Auger electrons produced by the interaction of the x-ray beam with the materials in the sample chamber. Most of these electrons have energies of 1 keV or more;[16] we call them primary electrons. Primary-electron emission can contribute an extraneous signal if the number of primary electrons emitted onto the sample electrodes from surfaces in the sample environment is different from the number of primary electrons emitted from the electrode surfaces back into the environment. Even if the electrodes and the windows are of the same material it is possible to get a signal from the primary electrons due to sample chamber geometry and the manner in which the electrical connections are made.

We were able to minimize the signal due to primary-electron emission by covering all exposed surfaces with beryllium foil and electrically connecting the front electrode of the sample to the inner chamber by a low-inductance path. X-ray-induced charge emission from fairly pure beryllium at kiloelectron-volt energies is very small - of the order of 10^3 less than the emission from medium- and high-Z materials. In the front part of the chamber, the use of high-purity beryllium kept primary-electron emission to a minimum, and the low-inductance return path prevented these electrons from contributing to the signal. Extraneous currents did not flow in the rear part of the chamber because the x-ray beam was absorbed in the beam stop; thus, no electrons were emitted in this part of the chamber.

The other component of electron emission that can drastically affect the photoconductivity signal consists of secondary electrons. These low-energy (less than 50 eV) electrons are emitted whenever a primary electron exits from or enters a surface. Secondary electrons are particularly troublesome in photoconductivity experiments because they produce a bias-dependent signal that is difficult to extract from the photoconductivity signal. The procedures we used to eliminate the primary-electron signal were also effective in minimizing the signal due to secondary electrons.

The critical test of the sample environment is the size and character of the signals due to currents other than photocurrents. We measured these background signals by exposing a sample whose photoconductivity signal was inherently small. Under the assumption that the photoconductivity signal is inversely proportional to sample thickness, we chose a sample of polyethylene 1.25 mm thick. As we shall see, the background signals are very small

(1.3 mV for polyethylene) and are associated with charge transport in the insulating sample; so the effect of extraneous currents on our photoconductivity signals is negligible.

Some investigators have used three-layer samples or accordion-folded samples as a means of eliminating signals due to secondary electrons. We chose to retain the simpler parallel-plate geometry because we wanted to conduct future experiments on photon-induced charge transport in dielectric layers themselves. The parallel-plate geometry also makes it possible to construct realistic experimental models of flat cables.

Electrical Measuring Circuit

The signal from the sample was recorded by an oscilloscope that was connected to the sample with triaxial cable, as shown in Fig. 3. The center conductor of the cable was connected to the rear sample electrode. This electrode was biased at $\pm V_0$ with respect to ground. The inner braid of the cable, maintained at ground potential, was connected to the front electrode of the sample and to the inner chamber. The outer braid of the cable was connected to the outer chamber. The inner and outer braids were tied together at the oscilloscope chassis. We applied the sample bias voltage through another triaxial cable, as shown in Fig. 3. The triaxial cables were each placed within an additional shield, which was tied to the triaxial outer shield at the outer chamber and grounded near the oscilloscope.

We obtained the photoconductivity of the sample by measuring the voltage change across the parallel combination of R_1 and the 50 Ω impedance of the cable. This change in voltage, $V_R(t)$, was measured as a function of sample bias, V_0. Details of the solution of the circuit equations are considered below.

The sample was biased through a 47-ft length of triaxial cable. One end of the cable was connected to a dc power supply; the other end was connected as shown in Fig. 3. The RC time constant of the biasing circuit was 20 msec, so the biasing power supply and cable were effectively decoupled from the sample during the microsecond times in which the measurement is made.

The signal cables were triaxial cables 45 ft long. It was necessary to locate the oscilloscope and sample bias power supply outside the vault where the generator was located because of the intense electrical noise and possible radiation hazard inside the vault. Electrical noise during a generator pulse was less than 0.5 mV.

The signal cables were terminated in 50 Ω at a dual-beam oscilloscope. The plug-ins used for each channel were differential amplifiers. The bandwidth of this system was 50 Mhz, which corresponds to a 7 nsec risetime limitation. We set the sweep rates of the two beams at 20 nsec/cm when we were correlating the photoconductivity and dose-rate signals.

Figure 5 shows oscillograms typical of the experimental data from three materials. The lower beam recorded the charge-emission signal from the beryllium foil, which was used as a dose-rate monitor, and the upper beam recorded the photoconductivity signal. We operated the plug-ins in the differential (A-B) mode and fed a common fiducial signal into the B channel of both beams. The fiducial pulse originated from an external trigger output on the oscilloscope and was adjusted so that it appeared near the end of the trace record. After making a correction for a slight lower-beam-sweep nonlinearity, we were able to correlate the upper and lower beam sweeps within ±1.5 nsec.

Electrical Circuit Analysis

Figure 6 shows the equivalent circuit used in the analysis of the photoconductivity signals. The dielectric sample during and after irradiation is represented by a fixed capacitance, C_S, shunted by a time-varying resistance, $R_S(t)$. In our analysis, C_S includes the stray capacitance of the measuring circuit. The resistance R is the load resistance across the sample. In the actual measuring circuit, R was the parallel combination of the 12-Ω resistor in Fig. 3 and the 50-Ω characteristic impedance of the cable, giving a net load resistance of about 10 Ω. $V_R(t)$ is the voltage across this load as observed on the oscilloscope. The sample-biasing capacitor has been replaced by a battery with terminal voltage V_0, since the capacitance of the sample-biasing capacitor is so large that its voltage does not change appreciably during the time of measurement.

We wish to derive an expression relating the resistance of the sample, $R_S(t)$, to the voltage, $V_R(t)$, observed on the oscilloscope. The analysis of the circuit in Fig. 6 proceeds as follows: By Kirchhoff's laws,

$$i_3 = i_1 + i_2 \tag{21}$$

$$i_1 = \frac{V_R(t)}{R} \tag{22}$$

$$i_2 = C_S \frac{dV_S(t)}{dt} = -C_S \frac{dV_R(t)}{dt} \tag{23}$$

$$i_3 = \frac{-V_R(t) + V_0}{R_S(t)} . \tag{24}$$

Substituting Eqs. (22), (23), and (24) into Eq. (21) we obtain

$$R_S(t) = \frac{V_0 - V_R(t)}{\frac{V_R(t)}{R} + C_S \frac{dV_R(t)}{dt}} , \tag{25}$$

In our experiments, the measured signal, $V_R(t)$, is completely negligible compared with the bias voltage, V_0; thus,

$$R_S(t) = \frac{V_0}{\frac{V_R(t)}{R} + C_S \frac{dV_R(t)}{dt}} . \tag{26}$$

We obtain the photoconductivity, $\sigma_s(t)$, from the relation

$$\sigma_s(t) = \frac{\ell}{R_S(t) A_r} , \tag{27}$$

where ℓ is the sample thickness, A_r is the irradiated area of the sample, and $R_S(t)$ is determined by Eq. (26). In simple, parallel-plate geometry, this expression may be rewritten as

$$\frac{\sigma_s(t)}{kk_0} = \frac{1}{R_S C_r} , \tag{28}$$

where C_r is the capacitance of the irradiated portion of the insulating sample, k_0 the permittivity of free space, and k the dielectric constant (measured at approximately 10 MHz). The conductivity divided by kk_0 is referred to as the normalized conductivity.

The quantity $C_S\ dV_R(t)/dt$ is small compared with $V_R(t)/R$. The derivative term expresses the fact that the rate of recharging the sample capacitance

through the load resistance R is finite, compared with the rate of change of the radiation pulse. The capacitance C_S is less than 1000 pF, even for the thinnest samples. We studied the response of the circuit in Fig. 6 by simulating $R_S(t)$ in a computer code. We made the time variation of $R_S(t)$ similar to the radiation pulse and compared the circuit response with $C_S = 1000$ pF to the ideal circuit response (with $C_S = 0$). We also included the actual circuit series inductance of 0.055 μH in these calculations. The only significant effect of the capacitance was to delay $V_R(t)$ with respect to the ideal response by about 10 nsec, the RC_S time constant.

To time-correlate the monitor and sample signals the response of the two circuits must be identical. We accomplished this by adding external capacitance to the monitor circuit so that it was electrically equivalent to the sample circuit.* The inductance of both circuits was the same, 0.055 μH. Under these circumstances both the monitor and sample signals lag the ideal response by the same time increment and these signals may be compared directly. Therefore, we neglected the integrating effect of C_S in calculating the conductivity, and Eq. 26 reduced to

$$R_S(t) = R \frac{V_0}{V_R(t)} . \tag{29}$$

Confining our attention for the moment to the peak of the observed signal (at $t = t_p$), we obtain from Eq. (29)

$$V_R(t_p) = \frac{R}{R_S(t_p)} V_0 . \tag{30}$$

*The monitor circuit is similar to the sample circuit in Fig. 6 except that a current generator replaces the varying resistance R(t).

This expression points out two very important aspects to be expected of a genuine photoconductivity signal (to the extent our model is valid). First, Eq. (30) predicts a linear dependence of the measured peak signals on sample bias voltage. Our experimental data for peak V_R when plotted against bias voltage should fit a straight line. Second, Eq. (30) predicts

$$V_R(t_p) \propto \frac{1}{\ell} , \tag{31}$$

where ℓ is the sample thickness. Measured peak signals may be expected to follow Eq. (30) as the dielectric sample thickness is varied (so long as the bulk properties of the thin and thick samples are the same).

For the measurement of peak induced conductivity Eqs. (28) and (30) yield

$$\frac{\sigma_s(t_p)}{kk_0} = \frac{1}{RC_r} \frac{V_R(t_p)}{V_0} . \tag{32}$$

We see that the peak normalized conductivity is determined by the capacitance of the irradiated portion of the sample and the slope of the sample-signal-vs-bias curve.

The photoconductivity at any time during and after the radiation pulse was obtained from the experimental data by a circuit analysis code that calculated the conductivity of the sample approximately every 2 nsec, using Eqs. (28) and (29). The photoconductivity and monitor signals were normalized and plotted on a common time axis. A fiducial mark ensured accurate time correlation – estimated as ±2 nsec for relatively smooth signals.

Sample Fabrication

The dielectric samples used in the photoconductivity measurements were films of polyethylene, polytetrafluoroethylene (hereafter called fluorocarbon), polyethylene terephthalate (hereafter called terephthalate), polyimide, epoxy, and glass. Table 1 summarizes the properties of these sample materials. Film thicknesses ranged from approximately 0.05 to 1.25 mm. The dielectric films were initially cleaned by ultrasonic agitation in trichlorethylene at 140°F. They were mounted between polystyrene rings that supported the edges of the sample.

Figure 7 is a sketch of the sample configuration. The electrode was shaped like a wheel with four spokes. The disk-shaped portion (3-cm diam) of the plating is slightly larger in diameter than the collimator (2.67-cm diam). The thin, evaporated electrodes were covered by beryllium, as shown in Fig. 3. The beryllium minimized the charge transfer between the sample and its environment and also served as electrical contact to the evaporated electrode. The raised center section of the rear beryllium disk compression-loaded the sample against the collimator in front. Clamps around the periphery of the sample, collimator, and beam stop ensured good electrical contact at the ends of the four electrode spokes.

Aluminum electrodes were vacuum deposited on the insulating films after the films were mounted in the plastic rings. Before electrode deposition the surface of each sample was further cleaned in the vacuum chamber by bombarding the surface with low-energy electrons or ultraviolet radiation. For most samples the aluminum electrodes were 1000 Å thick. The aluminum electrode thickness was varied between 500 and 2500 Å for the fluorocarbon and

terephthalate samples to study the effect of electrode resistance on the observed signals. We chose these thicknesses, which are substantially less than an electron range for 7-keV photoelectrons, so that the electrodes did not appreciably enhance the dose deposited in the dielectric material. If thick electrodes of medium- or high-Z material were used, emission of photoelectrons from the electrode material across the interface could substantially increase the radiation dose in the dielectric material next to the electrodes.

RESULTS

A major concern in the initial stages of our investigation was to assure ourselves that we were observing conduction effects in the bulk of our thin samples and not effects due to currents flowing exterior to them. Our understanding of the photoconductive process led us to expect certain behavior of the experimental data. In particular, for a given dose rate we expected the photocurrent to vary linearly with sample bias and to be inversely proportional to sample thickness, as predicted by Eq. (30). We also felt it was of the utmost importance to determine any contributions to the signal from sources other than photocurrents.

Figure 8 shows our measured peak photoconductivity signals plotted as a function of sample bias voltage for the six materials investigated. Data from two thicknesses of insulating film are shown for all the samples except glass and epoxy. The magnitude of these peak signals varies by a factor of about 100: from -8 mV in epoxy at +2500 V to about -700 mV in fluorocarbon at the same bias voltage. Since the oscilloscope signal, $V_R(t)$, is directly

proportional to the photocurrent through the sample, Fig. 8 shows that the peak photocurrents vary linearly with the sample bias voltage for all of the samples tested, so long as the magnitude of the electric field in the sample is less than approximately 2×10^5 V/cm. At higher fields, deviations from ohmic behavior are apparent in terephthalate, polyimide, and polyethylene. We will discuss this non-ohmic behavior later.

Comparison of the data from different thicknesses of sample (see Fig. 8) shows that the photocurrents are inversely proportional to the sample thickness to within about 10% for polyimide, 20% for fluorocarbon and terephthalate, and 30% for polyethylene. The agreement with Eq. (30) is within the experimental uncertainty, particularly when one considers that the samples of different thicknesses may have come from different batches of the parent material and may have been subject to different manufacturing processes.

Background effects, discussed earlier, were investigated by using thick samples of polyethylene. Figure 9 is a plot of the signal measured in a 1.25-mm-thick sample of polyethylene as a function of bias voltage. After we applied a small correction for photoconductivity (estimated from the thin polyethylene sample data) to this data, we found that the remaining signal was a constant, independent of bias. This bias-independent signal is very small – approximately 1.3 mV – and is identical to the zero-bias signal observed in the thin polyethylene sample (see Fig. 6). When the beam stop was placed in front of the sample the background signal was reduced to 0 ± 0.5 mV. We believe that photon induced charge transport within the dielectric is the source of the bias-independent signal observed from the thick polyethylene sample as well as of the signal observed from the thin

polyethylene samples at zero bias. We feel that the effect of extraneous currents on our photoconductivity measurements is negligible. In computing the photoconductivity of a given sample we add to the experimental voltage, $V_R(t)$, a small correction equal in magnitude to the zero-bias signal observed in that sample.

The peak dose rate was varied by increasing the distance between the x-ray source and the sample. We found that the photoconductivity varied approximately linearly with dose rate over the very limited range from 9×10^8 to 7×10^9 rads/sec (air).

Figure 10 shows the photoconductivity signal from each of the materials tested (except epoxy) as a function of time for 500 nsec after the onset of the radiation pulse. The most striking feature of these traces is the great difference in the behavior of the photoconductivity from material to material immediately after the exciting radiation pulse. The glass sample shows no observable delayed conductivity, while the rest of the samples show varying degrees of delayed conductivity. The polyethylene sample shows a small component of delayed conductivity with a decay time of about 50 nsec. The terephthalate, polyimide, and fluorocarbon samples show delayed conductivities with longer decay times; and the magnitude of the delayed signal relative to the prompt signal in these materials depends on the electric field. The ratio of the delayed signal (measured 50 nsec after the peak) to the peak signal in the thin terephthalate and polyimide samples increases from approximately 8% at 500-V bias to 30% at 2500-V bias.

We were particularly interested in making a detailed comparison of dose rate and photoconductivity in the samples. Figure 11 shows the induced

conductivity and dose rate signals plotted on the same time axis for fluorocarbon, terephthalate, polyimide, and polyethylene at a bias voltage of 1500 V. The photoconductivity was obtained from a plot of the experimental data by a circuit analysis code that calculated the conductivity of the sample approximately every 2 nsec using Eqs. (28) and (29). The time response of the monitor circuit was made identical to that of the sample circuit.

All the samples except glass show an induced conductivity of longer duration than the exciting radiation pulse. The photoconductivity in glass is in phase with the radiation throughout the duration of the pulse, while for polyimide and terephthalate the photoconductivity is in phase with the radiation only during the rising portion of the pulse. The photoconductivity and dose rate peak at about the same time (within an experimental uncertainty of ±2 nsec) in terephthalate, polyimide, and glass, while the peak photoconductivity lags the peak dose rate by approximately 5 nsec in fluorocarbon. As the bias voltage is decreased the photoconductivity comes more nearly into phase with the exciting radiation in all of the sample materials.

Table 2 summarizes the results of the photoconductivity measurements. We obaerved no polarization (charge buildup) or surface effects in any of the data. Varying the thickness of the aluminum electrodes over the 500 to 2500 Å range and pretreating the dielectric surface with electron bombardment and/or ultraviolet exposure before vacuum deposition produced no significant difference in signal magnitude or shape. The rear sample electrode was removed from one of the terephthalate samples so that the beryllium surface of the beam stop served as the electrode. The photoconductivity data recorded from this sample was identical with that from the two-electrode samples.

DISCUSSION

The lack of polarization and surface effects in these experiments is not surprising, since the maximum charge that flowed through any of the samples during a x-ray pulse was only about 0.05% of the charge stored on the sample electrodes. Even if the electrodes provided completely blocking contracts, we would not expect to observe polarization effects at our dose levels.

The time dependence of the photoconductivity relative to the dose rate can be qualitatively explained on the basis of the simple model described here. If we assume it takes 15 eV, on the average, to make an electron-hole pair in the insulating films, a total dose of 100 rads would result in the excitation of approximately 4×10^{14} electrons/cm^3. This number represents the maximum number of free carriers (n_c) or trapped carriers (n_t). As discussed earlier, trap densities, N_t, are believed to be at least 10^{18} cm^{-3} in amorphous and polymeric materials; and, since n_t cannot exceed the total number of carriers generated, $N_t >> n_t$. The effective density of states in the conduction band, N_c, is of the order of 10^{19} cm^{-3}; so, $N_c >> n_c$. Under these conditions we can rewrite Eqs. (14) and (15) as

$$\frac{dn_c}{dt} = g(t) - k_1 n_c + k_2 n_t - \alpha_3 n_c (n_c + n_t) \tag{33}$$

$$\frac{dn_t}{dt} = k_1 n_c - k_2 n_t, \tag{34}$$

where

$$k_1 = \alpha_1 N_t \text{ and } k_2 = \alpha_2 N_c \ . \tag{35}$$

The generating function, g(t), was taken to be a Gaussian function with a 40 nsec FWHM and was normalized to a total excitation of 4×10^{14} carriers/cm^3. We solved Eqs. (33) and (34) numerically for various sets of rate constants. We used the values obtained for $n_c(t)$ to calculate the conductivity, assuming an electron mobility of 1 cm^2/V-sec (holes are immobile in our model). To obtain a peak conductivity consistent with the peak conductivity observed experimentally, the ratio of trapped to free carriers had to be made very large - of the order of 10^7. This was accomplished in the model by making $k_1/k_2 \gg 1$ in Eqs. (33) and (34).

A solution of Eqs. (33) and (34) that gives reasonable agreement with the experimental data is plotted in Fig. 12. For comparison purposes the conductivity measured in the thin terephthalate is also shown. The time dependence of the generating function used in the calculation was made identical to that of the dose rate during the sample exposure. The rate constants were $k_1 = 10^{12}$ sec^{-1}, $k_2 = 5 \times 10^6$ sec^{-1}, and $\alpha_3 = 10^{-4}$ cm^3/sec. The peak conductivity calculated using these rate constants is 1.6×10^{-9} $(\Omega\text{-cm})^{-1}$, which lies between the experimental values obtained for terephthalate and polyethylene. The time dependence of the conductivity and its relationship to the generation function, g(t), are similar to what is seen in the experimental data. The amount of delayed conductivity depends on the value of k_2; the value chosen for our example results in a delayed component typical of that observed in our samples.

We made several calculations to study the dependence of the induced conductivity on dose rate. We varied the carrier generation from 4×10^{12} to 4×10^{16} cm^{-3} while holding the generation time constant. The rate

constants, k_1 and k_2, were the same as those defined above. We found that the peak conductivity varied linearly over this entire range of generation rates, in agreement with our experimental observations.

One may ask if the values for the rate constants used in Eqs. (33) and (34) are reasonable. The cross sections for capture of a free electron by a Coulomb center are estimated to be 10^{-11} to 10^{-13} cm^2 (Ref. 4), while cross sections for capture at an uncharged center are estimated to be of the order of atomic dimensions ~ 10^{-15} cm^2. By reaction kinetics, the rate constant is the product of the cross section for trapping or recombination and the thermal velocity of the carrier. We can write from Eq. (35)

$$\sigma_1(\text{trap capture}) = k_1/vN_t \tag{36}$$

$$\sigma_3(\text{recombination}) = \alpha_3/v \ . \tag{37}$$

Using a value for the trap density of 10^{18} cm^{-3}, a k_1 value of 10^{12} sec^{-1}, an α_3 value of 10^{-4} cm^3/sec, and a thermal electron velocity, v, of 10^7 cm/sec, we find $\sigma_1 = 10^{-13}$ cm^2 and $\sigma_3 = 10^{-11}$ cm^2. These cross sections are consistent with those estimated for capture into Coulomb centers.

The value chosen for k_2 determines the depth of the trapping level in the model. We calculate a trap depth of about 1.0 eV from detailed balance considerations, using the trap capture cross section and density of states in the conduction level estimated above.

The field-dependent delayed conductivity observed in some of the materials may be qualitatively explained on the basis of the trapping model and the effect of the applied electric field on the energy levels in the model.

Similar field dependence of the conductivity observed in thin films of Ta_2O_5 and SiO has been explained in terms of field-assisted ionization of trapping levels in the dielectric (Poole-Frenkel effect). The Poole-Frenkel effect[17] is the interaction of the bias field with trapping centers in an insulator, which results in a lowering of the coulombic trapping barrier and a subsequent enhancement in the rate at which carriers are released from the traps into the conduction band. The barrier lowering is described by

$$\Delta\mathcal{E}_t = \beta_p E^{1/2} \tag{38}$$

$$\beta_p = 2(e^3/4\pi\, kk_0)^{1/2}\ , \tag{39}$$

where $\Delta\mathcal{E}_t$ is the effective decrease in the depth of the trapping level below the conduction band of the insulator, E is the electric field in the sample, e is the electronic charge, k is the dielectric constant of the insulator at optical frequencies, and k_0 is the permittivity of free space. At our maximum field of 5×10^5 V/cm, Eq. (38) predicts a barrier lowering of 0.31 eV. This increases the value of the parameter k_2 by five orders of magnitude above the low field value.

Figure 13 shows solutions of Eqs. (33) and (34) for different values of k_2. While the model is too simple to predict detailed behavior, it does show the same qualitative behavior with field strength (trap depth) as some of the experimental data. Since the Poole-Frenkel effect occurs only for coulombic trapping centers, the large values we estimate for the trapping cross sections lend further support to our interpretation of the field-dependent delayed conductivity data.

The somewhat faster than linear increase of peak conductivity with bias voltage in the terephthalate and polyimide samples may also be due, in part, to the field dependence of the conductivity. The trapping model exhibits a similar increase in peak conductivity when the rate of emission from the traps is increased (see Fig. 13). In the case of polyethylene, which did not show a field-dependent delayed conductivity, the nonlinearity may be due to a prebreakdown effect, since the peak electric field approached the breakdown field in this material.

The behavior of fluorocarbon is more complex. This material exhibited no nonlinearity in the peak signal, even though its ratio of delayed current to peak current was larger than that of any of the other materials.

Figure 14 compares our measurements with those of other investigators. Our data are plotted at the peak dose rates achieved in the particular sample material. We believe this is also true for the data from the other investigators. The TREE data, extrapolated to higher dose rates, are consistently higher than our measurements – by several orders of magnitude in the case of fluorocarbon and polyimide. Better agreement exists between our results and recent Sandia measurements[18] when the latter are extrapolated to lower dose rates.

SUMMARY

- X-ray-induced photocurrents obey Ohm's law to fields of about 5×10^5 V/cm in epoxy, glass, and fluorocarbon. At fields greater than about 2×10^5 V/cm, terephthalate, polyimide, and polyethylene photocurrents increased at a slightly faster than linear rate with electric field.

- Measured photocurrents varied approximately as (thickness)$^{-1}$, indicating a bulk effect.
- All samples except glass showed some "delayed" photoconductivity; i.e., the fall in conductivity lagged the fall in the radiation pulse. Fluorocarbon showed the largest conductivity immediately after the radiation pulse, while epoxy and polyethylene showed the smallest components (no larger than 10%). Terephthalate and polyimide showed measurable (~1% peak) conductivity to times about 100 μsec after the radiation pulse. The magnitude of this delayed conductivity increased with increasing electric field in terephthalate, polyimide, and fluorocarbon, an effect that is consistent with some type of field-assisted carrier generation.
- Charge displacement signals are small (<12 mV) and vary about as expected with the atomic number of the material.
- The magnitude and time dependence of the conductivity signals are qualitatively described by a simple solid-state trapping model, using reasonable values for mobility, trap density, capture cross sections, and trap depths.

ACKNOWLEDGMENTS

The mechanical engineering for this program was provided by R. Waldron. Numerical calculations on the solid-state physics model were performed by A. Ciplickas. The dielectric samples were fabricated under the direction of G. Scott at Bendix Crop., Kansas City, Missouri.

REFERENCES

1. R. Weingart, R. Barlett, and R. Lee, Lawrence Livermore Laboratory, Internal report (1970). Readers outside the Laboratory who desire further information on LLL internal documents should address their inquiries to Technical Information Department, Lawrence Livermore Laboratory, Livermore, California 94550.
2. *TREE (Transient-Radiation Effects on Electronics) Handbook*, 2nd ed., Battelle Memorial Institute, Columbus, Ohio, Rept. DASA-1420-1 (1969). This document has been superseded, and copies of the older editions may no longer be in circulation.
3. C. Kittel, *Introduction to Solid State Physics*, 3rd ed. (John Wiley & Sons, Inc., New York, 1960).
4. R. Bube, *Photoconductivity of Solids* (John Wiley & Sons, Inc., New York, 1960).
5. A Rose, *RCA Rev.* **12**, 362 (1951).
6. A Rose, *Concepts in Photoconductivity and Allied Problems* (Interscience Publishers, Inc., New York, 1963).
7. J. F. Fowler, *Proc. Roy. Soc. London* **A236**, 464 (1956).
8. A. I. Gubanov, *Quantum Electron Theory of Amorphous Semiconductors* (Consultants Bureau, New York, 1965).
9. L. Banyai, *Physique des Semiconducteurs* (Dunod, Paris, 1964), p. 417.
10. N. F. Mott, *Phil. Mag.* **19**, 835 (1970).
11. F. Gutman and L. Lyons, *Organic Semiconductors* (John Wiley & Sons, Inc., New York, 1967).

12. L. I. Maissel and R. Glang, *Handbook of Thin Film Technology* (McGraw-Hill Book Company, Inc., New York, 1970), p. 14-15.

13. A. Blumlein, British Patent 589127.

14. V. W. Slivinsky, Lawrence Livermore Laboratory, internal report (1970).

15. P. J. Ebert, J. L. Gaines, and G. R. Leipelt, *Nucl. Instrum. Methods* 99, 29 (1972).

16. E. P. Denisov, *et al.*, *Sov. Phys. Solid State* 6, 2047 (1965).

17. J. Frenkel, *Phys. Rev.* 54, 647 (1938).

18. W. H. Sullivan and R. S. Ewing, *IEEE Trans. Nucl. Sci.* NS-18, 310 (1971).

Table 1. Properties of sample materials.

Material	Peak dose rate[a] (rads/sec)	Dielectric constant	Elemental composition (approx)	Capacitance (pF)	Resistivity (Ω-cm)
Polyethylene (high density	2.4×10^9	2.26 (60 Hz-100 GHz)	CH_2	230	$\sim 10^{17}$
Polytetrafluoroethylene (Teflon FEP)	9.5×10^9	2.1 ± 0.1 (100 Hz-100 MHz)	CF_2	185	$\sim 10^{17}$
Polyethylene terephthalate (Mylar A)	4.4×10^9	3.0 (1 MHz)	$C_{12}H_5O_5$	291	$\sim 10^{18}$
Polyimide (Kapton)	4.7×10^9	3.45 (10 MHz)	$C_{22}H_5O_{10}N_2$	335	$\sim 10^{18}$
Epoxy (100/20 Epi-Rez 510 Epoxy/Epoxy Curing Agent)	3.5×10^9	3.60 (10 MHz)	$C_{30}H_{34}O_5N$	367	$\sim 10^{16}$
Glass (borosilicate)	5.9×10^{10}	6.7 (1 MHz)	$Si_{10}O_{26}B_8KZ_n$	406	$\sim 10^{16}$

[a]Corresponds to about 7×10^9 rads/sec in air.

Table 2. Photoconductivity data. The peak conductivity tabulated here is obtained from the slope of the linear portion of the sample-signal-vs-bias curve using Eq. (32). The magnitude and decay time of the delayed conductivity was obtained at 2 kV bias voltage. The decay time is defined as the time for the conductivity persisting at the end of the radiation pulse to decay to half its value. Some samples showed small delayed components of conductivity of much longer duration than those tabulated here.

Material	Peak dose rate (rads/sec in material)	Peak conductivity (mho/F)	Conductivity at end of radiation pulse (50 nsec after peak)	Decay time of conductivity (nsec)
Polyethylene terephthalate	4.4×10^9	3.2×10^3	$\sim 8 \times 10^2$	~150
Polyimide	4.7×10^9	1.8×10^3	$\sim 4.5 \times 10^2$	~90
Polyethylene	2.4×10^9	1.3×10^4	$\sim 2.3 \times 10^3$	~50
Polytetrafluoroethylene	9.5×10^9	1.6×10^5	$\sim 8 \times 10^3$	~150
Epoxy	3.5×10^9	7.4×10^2	<5% of peak	-
Glass	5.9×10^{10}	6.2×10^3	~0	-

FIGURE CAPTIONS

Fig. 1. Simple model of a photoconductor with trapping. Electrons are excited from the valence level to the conduction level at a rate g(t). We assume that the holes arising in the valence level from the electron excitation are immediately captured in the recombination level. The trapping level is close to the conduction level, and thus a thermal exchange of electrons takes place between the two levels. We assume that the trapped electrons communicate only with the conduction band and that the temperature is low enough that direct thermal excitation of carriers from the valence band to the conduction band may be neglected.

Fig. 2. X-ray spectrum incident on the sample. The spectrum from our generator consists of the tungsten L lines superimposed on a brehmsstrahlung spectrum. The low-energy cutoff (dashed line) arises from a composite beam filter of 1.5 mm beryllium and 0.025 mm aluminum located in front of the sample.

Fig. 3. Schematic diagram of sample chamber.

Fig. 4. Collimator and beam stop. The x rays are collimated by the aluminum and gold layers to the left of the sample. A similar laminate to the right absorbs all the x rays before they can strike the rear walls of the chamber. All exposed surfaces, as well as the sample interfaces, are covered with beryllium.

Fig. 5. Typical experimental waveforms. The upper trace of each pair is the photoconductivity signal, and the lower trace is the dose rate monitor signal. The sweep speed is 20 nsec/div. The bias voltage

is -2 kV for all three samples. The timing fiducials are not shown. Note how the photoconductivity signal from the glass sample follows the monitor signal.

Fig. 6. Equivalent circuit for the sample-chamber schematic shown in Fig. 3. The capacitance C_s includes the stray capacitance of the measuring circuit. V_0 is the bias voltage. R is the load resistance across which the measured voltage, $V_R(t)$, is generated.

Fig. 7. Insulating sample configuration. The insulating films were mounted between rings of polystyrene. A mask was used to obtain the metallized pattern in the vacuum deposition chamber.

Fig. 8. Measured peak photosignals as a function of sample bias voltage. Note the deviation from linearity in the case of thin samples of polyimide, terephthalate, and polyethylene.

Fig. 9. Variation of signal with bias voltage for a thick (1.25 mm) polyethylene sample. The solid line is the data from the sample, and the dashed line is the data from which the photoconductivity has been subtracted. The latter constitutes our background signal. The background is approximately constant (-1.3 mV), independent of bias voltage (the zero-bias signal was -1.3 mV).

Fig. 10. Photoconductivity as a function of time and bias voltage. The upper curve of each pair is the photoconductivity signal; the lower curve is the dose rate monitor signal. The units of the abscissae are in millivolts. The sweep for each curve is 50 nsec/div. Note the large differences in the magnitude of the photocurrents from material to material both during and after the radiation pulse.

Fig. 11. Comparison of photoconductivity and dose rate. The two are in phase for the glass sample, but the fall in conductivity lags the fall in dose rate for the other samples.

Fig. 12. Comparison of calculated and experimental conductivities. The measured conductivity is for the 0.055-mm terephthalate sample. The sample bias voltage was 1500 V. The dose rate measured during the sample exposure is also shown. The generation rate used in the calculation was made identical to the measured dose rate. The time dependence of the measured and the calculated conductivities agree closely.

Fig. 13. Dependence of free carrier density on trap depth. For values of k_2 no larger than 5×10^5 sec^{-1}, the time dependence of the free carrier density and the time dependence of the generation rate, g(t), are identical except for a very small tail at times longer than 100 nsec. As k_2 increases from 5×10^5 to 5×10^7 sec^{-1}, the ratio of the number of free carriers when the generation becomes negligible to the number near the peak generation rate increases from about 2% to 80%. The conductivity measured in several of the samples exhibited a similar behavior as the electric field was varied.

Fig. 14. Photoconductivity as a function of dose rate. The reference dose rate for the LLL data is the actual dose rate in the sample material. The spread in the measurements from which the TREE data was derived is about 100.

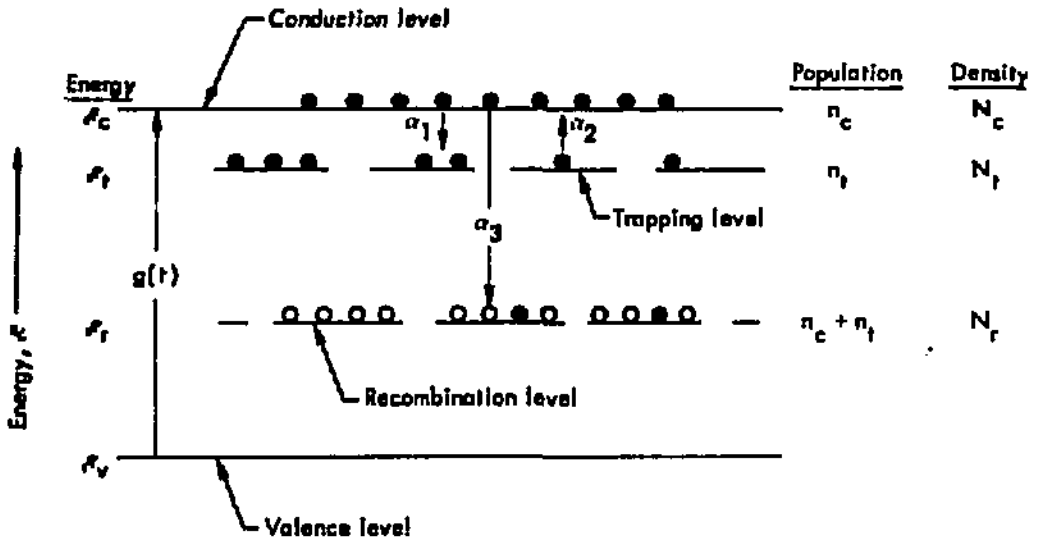

Weingart – Fig. 1

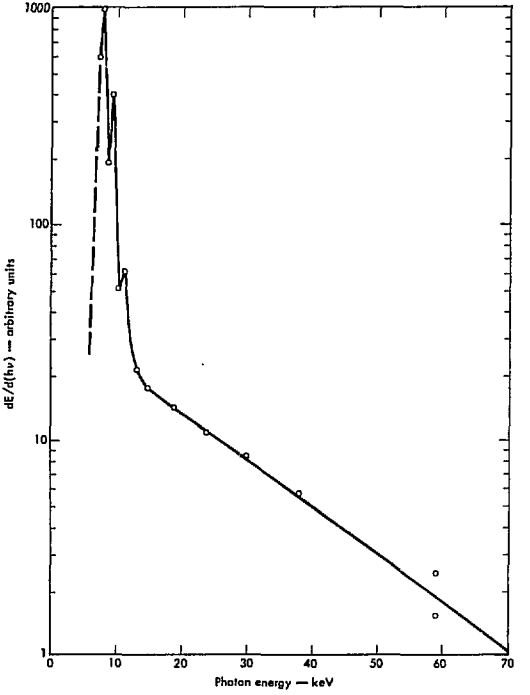

Weingart - Fig. 2

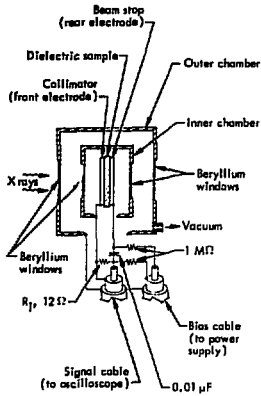

Weingart - Fig. 3

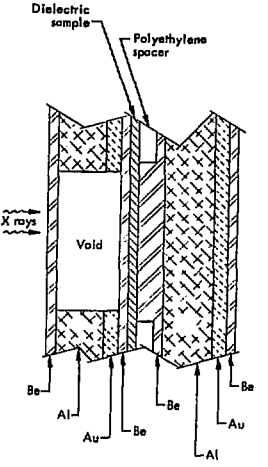

Weingart – Fig. 4

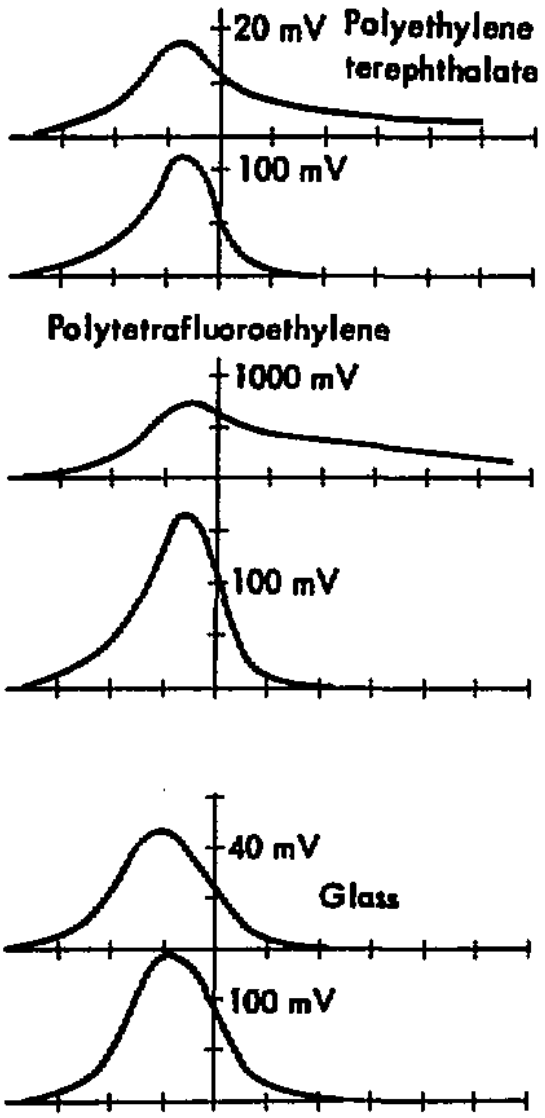

Weingart - Fig. 5

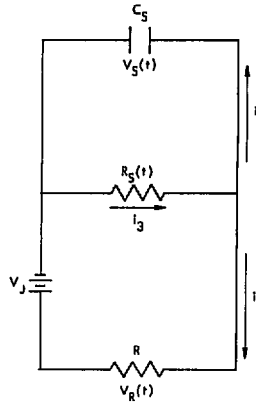

Weingart - Fig. 6

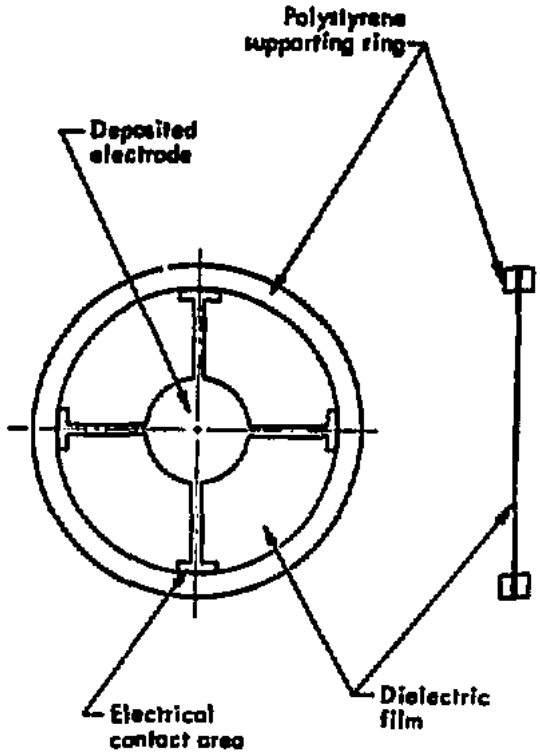

Weingart - Fig. 7

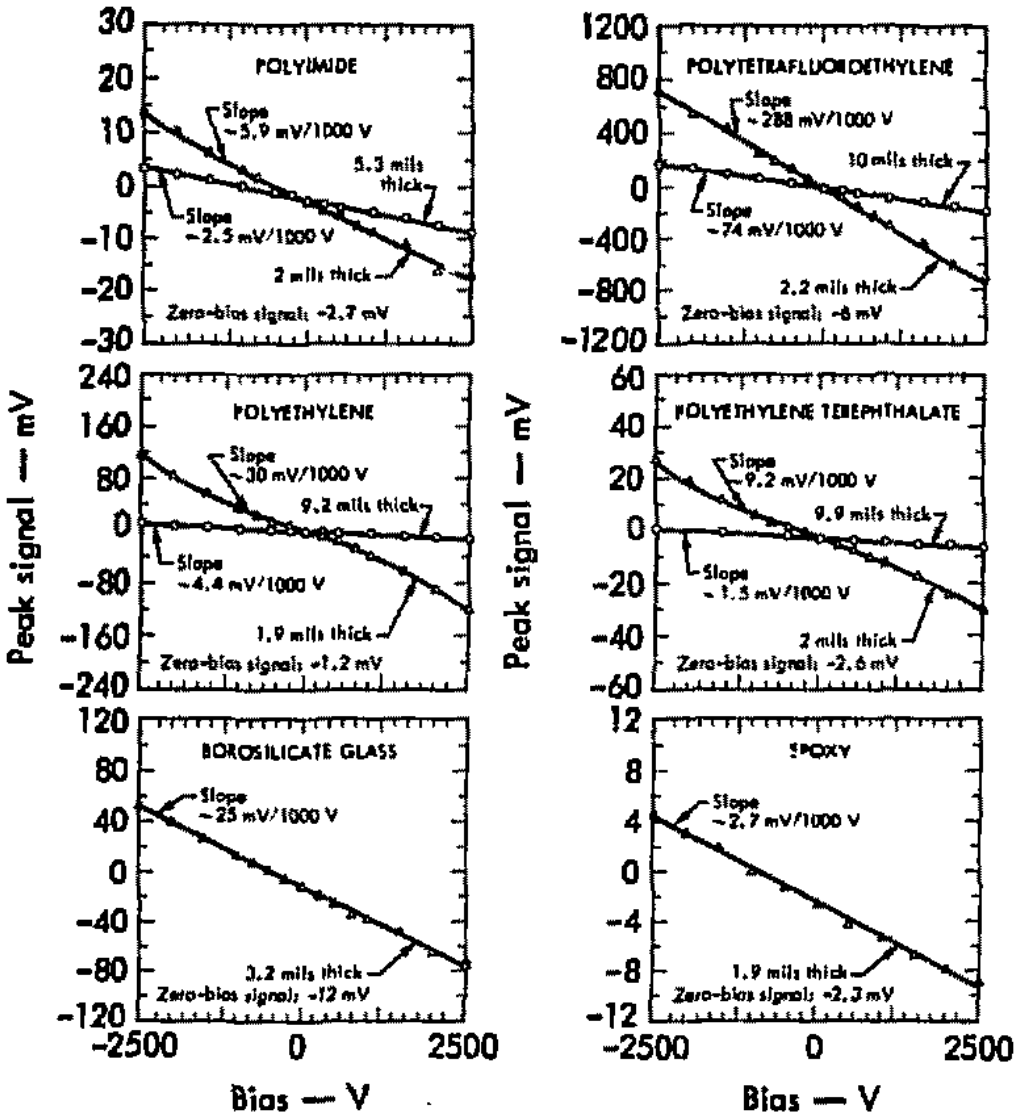

Weingart – Fig. 8

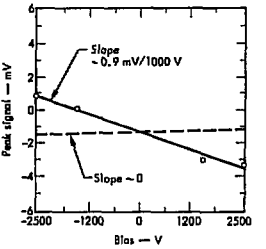

Weingart – Fig. 9

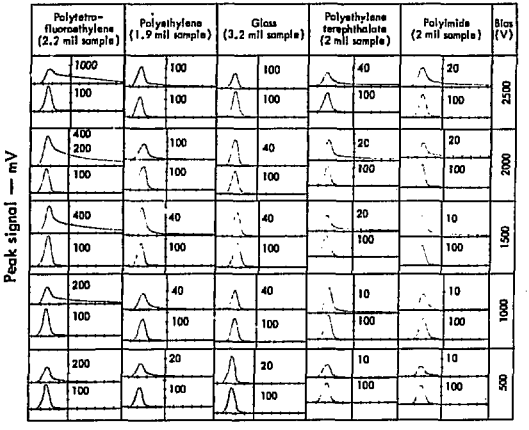

Weingart - Fig. 10

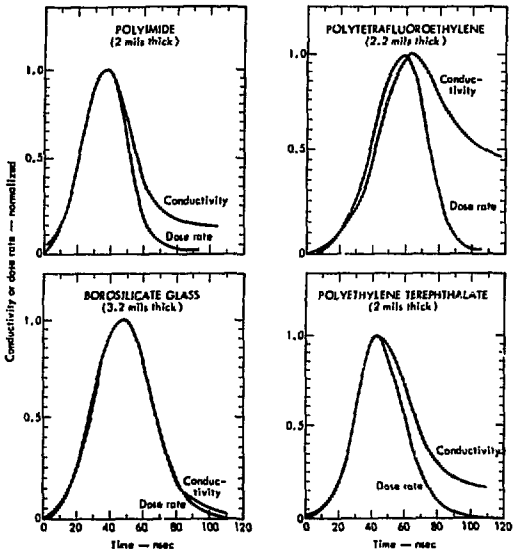

Weingart - Fig. 11

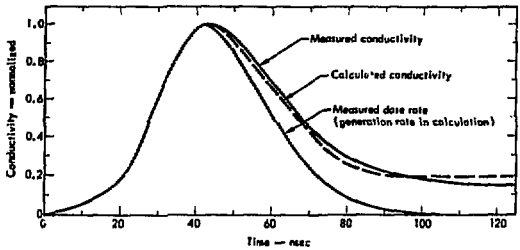

Weingart – Fig. 12

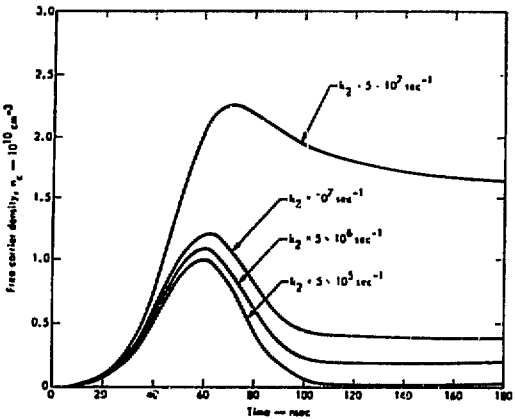

Weingart - Fig. 13

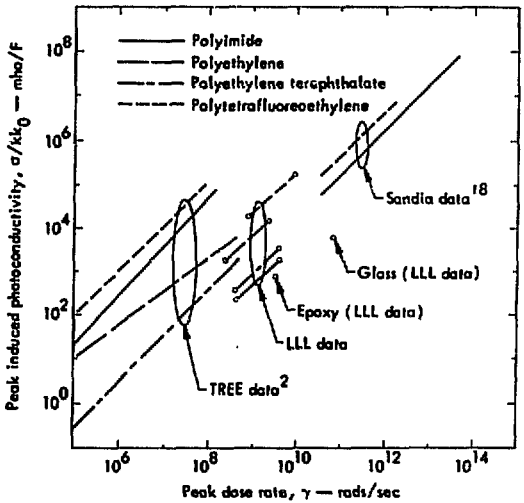

Weingart - Fig. 14